Alternative splicing results in RET isoforms with distinct trafficking properties

Douglas S. Richardson[a,*], David M. Rodrigues[b], Brandy D. Hyndman[a], Mathieu J. F. Crupi[a], Adrian C. Nicolescu[a], and Lois M. Mulligan[a]

[a]Department of Pathology and Molecular Medicine and Division of Cancer Biology and Genetics, Cancer Research Institute, Queen's University, Kingston, ON K7L 3N6, Canada; [b]Gastrointestinal Disease Research Unit, Kingston General Hospital, and Queen's University, Kingston, ON K7L 3N6, Canada

ABSTRACT ***RET*** **encodes a receptor tyrosine kinase that is essential for spermatogenesis, development of the sensory, sympathetic, parasympathetic, and enteric nervous systems and the kidneys, as well as for maintenance of adult midbrain dopaminergic neurons.** ***RET*** **is alternatively spliced to encode multiple isoforms that differ in their C-terminal amino acids. The RET9 and RET51 isoforms display unique levels of autophosphorylation and have differential interactions with adaptor proteins. They induce distinct gene expression patterns, promote different levels of cell differentiation and transformation, and play unique roles in development. Here we present a comprehensive study of the subcellular localization and trafficking of RET isoforms. We show that immature RET9 accumulates intracellularly in the Golgi, whereas RET51 is efficiently matured and present in relatively higher amounts on the plasma membrane. RET51 is internalized faster after ligand binding and undergoes recycling back to the plasma membrane. This differential trafficking of RET isoforms produces a more rapid and longer duration of signaling through the extracellular-signal regulated kinase/mitogen-activated protein kinase pathway downstream of RET51 relative to RET9. Together these differences in trafficking properties contribute to some of the functional differences previously observed between RET9 and RET51 and establish the important role of intracellular trafficking in modulating and maintaining RET signaling.**

Monitoring Editor
Thomas F.J. Martin
University of Wisconsin

Received: Feb 13, 2012
Revised: Jul 5, 2012
Accepted: Jul 31, 2012

This article was published online ahead of print in MBoC in Press (http://www.molbiolcell.org/cgi/doi/10.1091/mbc.E12-02-0114) on August 8, 2012.

*Present address: Department of NanoBiophotonics, Max Plank Institute for Biophysical Chemistry, 37077 Göttingen, Germany.

Address correspondence to: Lois M. Mulligan (mulligal@queensu.ca).

Abbreviations used: CBL, casitas B-lineage; CHX, cyclohexamide; Ct, crossing threshold; DRG, dorsal root ganglion; EEA1, early endosome antigen 1; EGFR, epidermal growth factor receptor; ENTH, epsin N-terminal homology domain; EPN1, epsin1; ER, endoplasmic reticulum; ERC, endocytic recycling compartment; ERK, extracellular-signal regulated kinase; FBS, fetal bovine serum; GDNF, glial cell line–derived neurotrophic factor; GFP, green fluorescent protein; GI, gastrointestinal; GFRα1, GDNF family receptors alpha 1; GRB2, growth factor receptor-bound protein 2; HEK, human embryonic kidney; HuD, Hu antigen D; LAMP2, lysosomal associated protein 2; MAPK, mitogen-activated protein kinase; MeSNa, 2-mercaptoethane sulfonate sodium; PNS, postnuclear supernatant; RA, retinoic acid; RET, rearranged during transfection; ROI, region of interest; RTK, receptor tyrosine kinase; SCG, superior cervical ganglion; SE, standard error; SHANK3, SH3 and multiple ankyrin repeat domains 3; SHC, SRC homology 2 domain containing transforming protein 1; STAT3, signal transducer and activator of transcription 3; TGN38, *trans*-Golgi network protein 38; TUB, tubulin; WT, wild type.

INTRODUCTION

The *RET* gene encodes a receptor tyrosine kinase (RTK) that is widely expressed in neuroendocrine tissues (reviewed in Arighi *et al*., 2005). *RET*-knockout mice are carried to term but die shortly after birth, displaying a lack of enteric innervation and kidney dysplasia (Schuchardt *et al*., 1994). In humans, a number of loss-of-function mutations have been identified throughout the *RET* gene that lead to Hirschsprung disease, a congenital disorder characterized by a loss of enteric neurons in the distal portions of the colon and small intestine (reviewed in Amiel and Lyonnet, 2001; Burzynski *et al*., 2009). Conversely, mutations that result in constitutively active receptors have been linked to tumors of various neuroendocrine tissues, including the thyroid, parathyroid, and adrenal glands (reviewed in Arighi *et al*., 2005; Lai *et al*., 2007). In addition, RET plays roles in spermatogenesis, development of the sensory, sympathetic, and parasympathetic nervous systems, and maintenance of adult midbrain dopaminergic neurons (Kramer *et al*., 2007; reviewed in Arighi *et al*., 2005).

Activation of RET occurs through the formation of a multimeric signaling complex consisting of RET's soluble ligand glial cell line–derived neurotrophic factor (GDNF) and a membrane-bound

Supplemental Material can be found at:
http://www.molbiolcell.org/content/suppl/2012/08/03/mbc.E12-02-0114.DC1.html

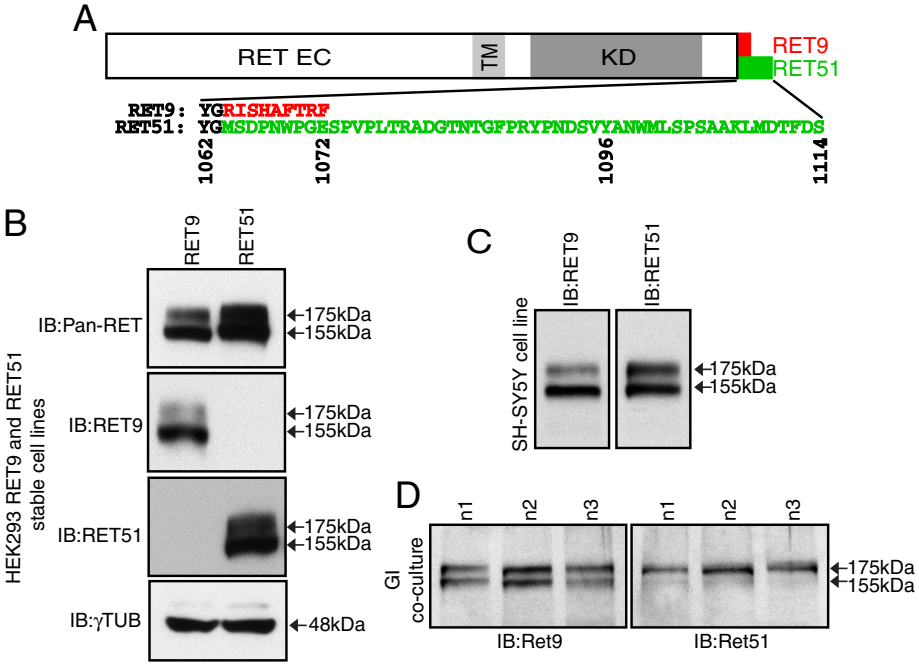

FIGURE 1: RET9 accumulates as immature protein. (A) Diagrammatic representation of RET9 and RET51. Amino acid sequences from tyrosine residue 1062 to the end of each isoform are presented. EC, extracellular domain; KD, kinase domain; TM, transmembrane domain. (B) Cell lysates from HEK293 cells stably expressing RET9 or RET51 were separated by SDS–PAGE and immunoblotted with pan-RET, isoform-specific RET9 or RET51, and anti–γ-tubulin antibodies. (C, D) Equal volumes of cell lysate from retinoic acid–treated SH-SY5Y neuroblastoma cells (C) or 4-d-old rat pup GI cocultures (D) that coexpress RET9 and RET51 were separated by SDS–PAGE and immunoblotted with RET9 or RET51 isoform-specific antibodies. n1–n3 represent GI cocultures established from three individual rat pups.

coreceptor, GDNF family receptor α 1 (GFRα1; reviewed in Airaksinen and Saarma, 2002). After ligand binding, RET initiates a number of downstream signaling cascades involved in cell growth, differentiation, proliferation, and migration, most notably phosphoinositide 3-kinase/AKT, extracellular-signal regulated kinase (ERK)/mitogen-activated protein (MAP) kinase, SRC, β-catenin, and STAT3 pathways (Besset *et al.*, 2000; Schuringa *et al.*, 2001; Encinas *et al.*, 2004; Gujral *et al.*, 2008).

The *RET* gene is alternatively spliced at its 3′ end to produce multiple protein isoforms. RET9 and RET51 are the most highly expressed and differ only in their 9 and 51 COOH-terminal amino acids, respectively (Figure 1A; Tahira *et al.*, 1990). In most tissues examined these isoforms are coexpressed; however, the *RET9* transcript is often expressed at much greater levels relative to *RET51* in human tissues (Ivanchuk *et al.*, 1998; Le Hir *et al.*, 2000; Lee *et al.*, 2003). Although the primary signaling hub shared by all RET isoforms is tyrosine 1062 (Asai *et al.*, 1996; De Vita *et al.*, 2000; Hayashi *et al.*, 2000), differences in the downstream amino acid sequences in RET9 and RET51, and the presence of an additional signaling hub in RET51 at Y1096 (Figure 1A; Besset *et al.*, 2000; Jain *et al.*, 2006), have been suggested to contribute to both signal redundancy between RET9 and RET51 and certain distinct properties of each of the isoforms. Each isoform can induce a unique autophosphorylation pattern on intracellular RET tyrosine residues and assemble a distinct complement of adaptor proteins (Tsui-Pierchala *et al.*, 2002). Specifically, RET9 and RET51 are known to differentially bind SHC, GRB2, c-CBL, and SHANK3 (Lorenzo *et al.*, 1997; Schuetz *et al.*, 2004; Scott *et al.*, 2005). Gene expression profiling revealed that RET9 and RET51 activity can induce overlapping but distinct gene expression patterns (Myers and Mulligan, 2004; Hickey *et al.*, 2009). Finally, in cell-based assays, RET51 possesses an increased intrinsic ability to transform cells and induce neurite outgrowth, potentially suggesting a higher level of signaling downstream of this isoform (Pasini *et al.*, 1997; Rossel *et al.*, 1997; Iwashita *et al.*, 1999; Le Hir *et al.*, 2000).

In vivo animal models have also shown differences in RET isoform functions. Mice that express monoisoformic mouse/human hybrid Ret9 ($Ret^{9/9}$ mice) or Ret51 ($Ret^{51/51}$) show distinct phenotypes (de Graaff *et al.*, 2001). $Ret^{9/9}$ mice are viable, whereas $Ret^{51/51}$ mice show kidney dysplasia and delayed development of the enteric nervous system (de Graaff *et al.*, 2001; Barlow *et al.*, 2003). Similarly, zebrafish expressing only ret9 protein formed an intact enteric nervous system, suggesting that ret51 is not required for this process (Heanue and Pachnis, 2008). In addition, it has been shown that the *RET51* transcript is not present until later stages of human development (Ivanchuk *et al.*, 1998), which may account for its dispensability in many of these studies. Overall, these data are consistent with the ability of RET9 and RET51 to influence both similar and distinct gene expression patterns downstream of their activation (Myers and Mulligan, 2004; Hickey *et al.*, 2009).

Exocytic trafficking of membrane proteins such as RTKs is complex and requires interactions with a host of proteins that target nascent peptides to the endoplasmic reticulum (ER), ensure their proper folding, mediate posttranslational modifications, and escort them to the plasma membrane (reviewed in Cross *et al.*, 2009). Once embedded in the plasma membrane, RTKs can bind extracellular ligands and become activated. Activation results in recognition of the RTK by the endocytic machinery of the cell, internalization, and targeting to intracellular structures for degradation or recycling back to the plasma membrane (reviewed in Maxfield and McGraw, 2004; Sorkin and von Zastrow, 2009). Thus, exocytosis and endocytosis are critical mediators of RTK subcellular localization. RTK signaling can be enhanced, directed toward or away from individual signaling pathways, or quenched, depending on the subcellular compartment in which it resides. Together mechanisms that direct RTK trafficking can have direct and profound effects on downstream signaling.

Although comprehensive studies of RET exocytosis and endocytosis are lacking, some insights into these processes have been provided. RET9 and RET51 are rapidly glycosylated within the ER to produce a 155-kDa immature glycoprotein (Takahashi *et al.*, 1991). Further processing occurs within the Golgi apparatus, resulting in expression of a fully glycosylated, mature, 175-kDa RET molecule on the plasma membrane (van Weering *et al.*, 1998). Previously, we showed that RET activation leads to rapid internalization and trafficking of the molecule to early endosomes, where it continues to activate downstream signaling pathways (Richardson *et al.*, 2006). The E3 ubiquitin ligase c-CBL can ubiquitinate RET, targeting the receptor for lysosomal degradation (Scott *et al.*, 2005; Richardson *et al.*, 2009), and a role for the proteasome in RET degradation has also been suggested (Pierchala *et al.*, 2006; Tsui and Pierchala, 2010).

Here, we present a comprehensive study of RET9 and RET51 subcellular localization and intracellular trafficking. We show that high levels of immature RET9 accumulate in the Golgi, whereas RET51 is efficiently matured and trafficked to the plasma membrane. In response to GDNF stimulation, both isoforms are targeted to the lysosome for degradation; however, RET9 appears to be targeted directly and efficiently, whereas a portion of RET51 molecules are recycled back to the membrane, making them available for continued signaling. Our data suggest that RET9 and RET51 possess distinct subcellular localizations and trafficking properties that help explain previously established isoform-specific downstream signaling characteristics.

RESULTS

RET51 matures more efficiently than RET9

Four cell-based model systems were used throughout this study. HEK293 cell lines transiently or stably expressing GFRα1 and either RET9 or RET51 (Myers and Mulligan, 2004) were used to analyze the individual contributions of these isoforms to intracellular processes (Figure 1B). SH-SY5Y neuroblastoma cells provide a model in which both RET9 and RET51 are expressed from *RET*'s endogenous promoter at higher levels relative to primary tissues (Figure 1C). HeLa cells transiently expressing RET9 or RET51 were well suited for direct visualization of intracellular trafficking by confocal microscopy due to their flat morphology and increased levels of RET expression relative to stable cell lines or cells endogenously expressing RET. Finally, a coculture model consisting of primary myenteric neurons, smooth muscle cells, and glia harvested from 4-d-old rats provided an endogenous system to which data from all other cell-based models could be compared (Figure 1D; Rodrigues *et al.*, 2011).

In initial investigations, we saw a marked difference in the relative distribution of the mature (175 kDa) and immature (155 kDa) protein forms of each RET isoform. In HEK293 cell lines stably expressing RET9 or RET51, mature and immature RET51 were expressed in nearly equivalent levels; however, RET9 appeared predominantly in the immature form (Figure 1B). Using isoform-specific antibodies for RET9 and RET51 (Supplemental Table S1), we noted a similar pattern of endogenous RET isoform expression in SH-SY5Y cells (Figure 1C) and an even more striking distribution in primary rat gastrointestinal (GI) cocultures, where immature Ret51 was nearly undetectable but equivalent amounts of both mature and immature Ret9 were observed (Figure 1D). Isoform-specific differences in mature protein expression, primarily decreased levels of mature RET9 protein, were most prominent in primary neurons, which had the lowest overall *RET* expression (Figure 1D), and least obvious in cells stably overexpressing *RET* (Figure 1B).

The glycosylation events that result in RET's maturation from 155 to 175 kDa have been shown to occur in the Golgi (Cosma *et al.*, 1998), suggesting that immature RET9 might accumulate in this region. We determined the localization of immature RET9 by immunofluorescence confocal microscopy in primary rat enteric neurons. In agreement with previously published data (Heanue and Pachnis, 2008; Rodrigues *et al.*, 2011), RET was expressed in Hu antigen D (HuD, ELAV4)–positive neurons but not the smooth muscle or glia of our GI coculture model (Supplemental Figure S1A). Despite low expression of *Ret* in these neurons (Figure 1D), we observed a region of Ret9 perinuclear accumulation that was not found in cells stained for Ret51 (Figure 2, A–C). Furthermore, the area enriched for Ret9 staining overlaid areas weak in HuD staining. HuD is a neuron-specific, mRNA-binding protein, primarily localized to the cytoplasm, where it interacts with ribosomes and is not expected to associate with perinuclear Golgi stacks (Burry and Smith, 2006), supporting the Golgi as the site of immature Ret9 accumulation. Consistent with this, we found that perinuclear Ret9 staining accumulates in and near structures harboring TGN38, a commonly used marker of the *trans*-Golgi network in rat cells (Supplemental Figure S1B; Ponnambalam *et al.*, 1996). We further investigated the localization of RET9 and RET51 in SH-SY5Y cells. As shown in Figure 2, D and E, both RET9 and RET51 could be seen in punctate structures near the plasma membrane. However, only RET51 was found to directly colocalize with EPN1-ENTH-green fluorescent protein (GFP), a marker of the inner leaflet of the plasma membrane (Ford *et al.*, 2002), in unstimulated cells. Together these results are consistent with our observations in Figure 1 and suggest that immature RET9 accumulates in the Golgi, whereas RET51 matures relatively more effectively, resulting in a greater plasma membrane presence of this isoform.

It was previously shown that *RET9* transcript is expressed at higher levels relative to *RET51* in multiple organisms and tissues (Ivanchuk *et al.*, 1998; Le Hir *et al.*, 2000; Lee *et al.*, 2003). Because *RET9* transcript levels appeared to correlate with the amount of immature RET9 protein in our various cell models (Figure 1, B–D), we investigated whether simple differences in *RET9* and *RET51* transcript expression could result in relatively more RET9 protein translation and an accumulation of immature RET9 in the ER and/or Golgi. Using quantitative real-time PCR, we confirmed that *RET9* transcripts are expressed at higher levels relative to *RET51* in SH-SY5Y cells and our primary rat GI cocultures (Figure 3A). HEK293 cell lines stably expressing monoisoformic RET9 or RET51 cDNA had similar levels of RET9 and RET51 transcripts, respectively (Figure 3A), likely due to their expression from the same promoter and lack of mRNA processing by the spliceosome. Of interest, despite similar transcript levels, a greater proportion of RET9 protein was still found in its immature form relative to RET51 in the HEK293 stable cell lines (Figure 1B), suggesting that higher transcript levels are not responsible for the accumulation of immature RET9. We confirmed this by performing a series of transient transfections in HEK293 cells in which we titrated the amount of transfected RET9 or RET51 plasmid DNA from 0 to 1 μg. As expected, decreases in transcript levels, by incrementally decreasing the DNA copy number delivered into cells, were unable to increase the amount of mature RET9 protein seen in Western blots (Supplemental Figure S2). Independent of transcript levels and the amount of nascent protein delivered to the ER, a number of chaperone proteins reside within the ER, Golgi, and cytoplasm to assist in protein folding, mediate posttranslational modifications, or delay export of misfolded and incorrectly modified proteins (Cross *et al.*, 2009). We did not expect that posttranslational processing at these sites would be responsible for the accumulation of immature RET9 because RET9 and RET51 possess identical extracellular domains—the region of RET located within the ER and Golgi during posttranslational processing. To confirm this, we compared Ret isoform maturation in primary rat GI cocultures grown at 30 and 37°C, as growth at reduced temperatures has been shown to improve maturation of difficult-to-fold proteins, including several RET mutants, that are retained in the ER and Golgi (Kjaer and Ibanez, 2003; Park *et al.*, 2009). Growth at 30°C did not affect the relative ratio of immature to mature Ret9 or Ret51 (unpublished data). Our observation that the pool of immature RET9 protein is maintained independent of RET DNA copy number within the cell and growth temperature suggests that the accumulation of immature RET9 is not due to either higher levels of RET9 transcript or less efficient folding or posttranslational modification of the protein, relative to RET51. Instead, it appears that the cell has an intrinsic ability to deliver RET51 to the plasma membrane, via the ER and Golgi, more efficiently relative to RET9.

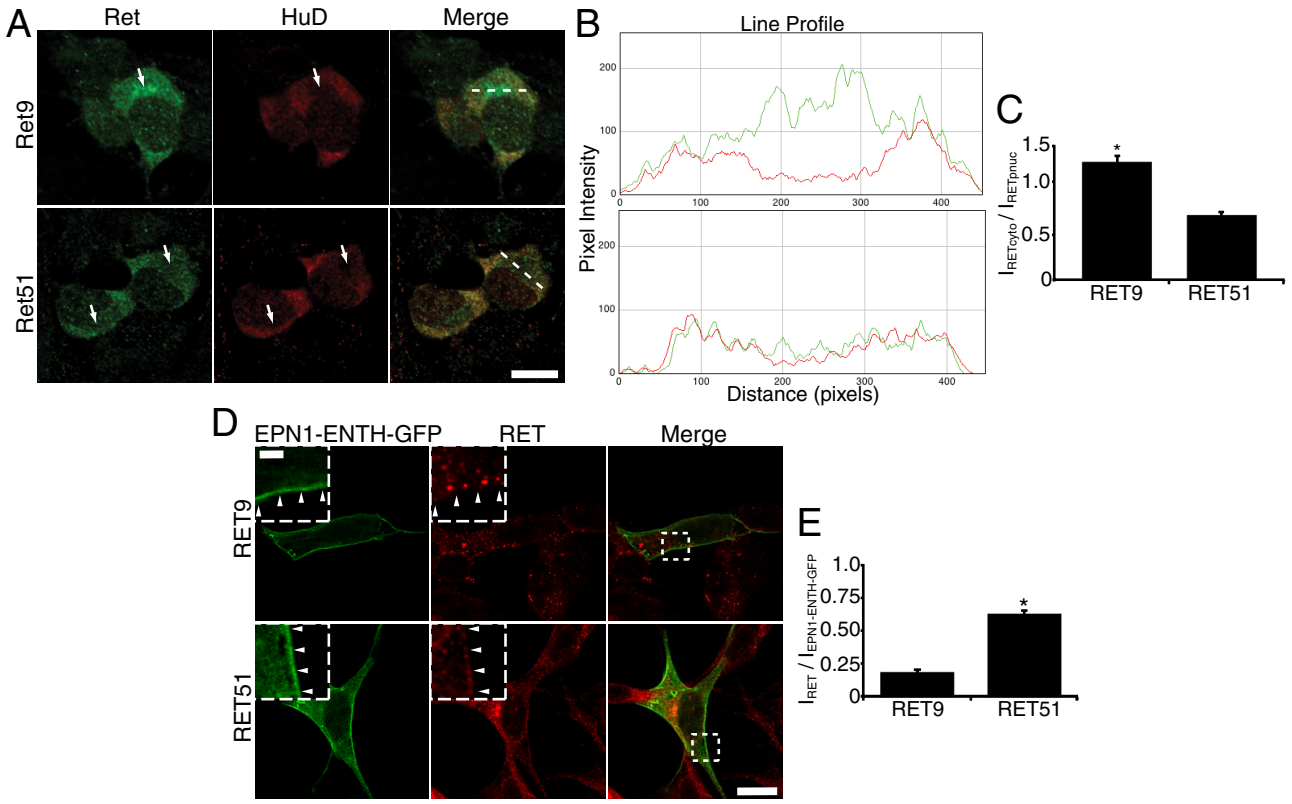

FIGURE 2: Immature RET9 accumulates in a perinuclear region. (A) GI cocultures were isolated from 4-d-old rat pups and plated on collagen-coated glass coverslips, grown for 60 h in 5% FBS, serum starved overnight, fixed, and stained for the neuronal marker HuD (red) and for Ret9 or Ret51 (green). Arrows highlight areas devoid of HuD staining. Scale bar, 40 μm. (B) Pixel intensity profiles were calculated along the dashed lines in the Merge panels of A and plotted. (C) Mean Ret9 or Ret51 signal intensity was calculated for two circular ROIs (a perinuclear ROI devoid of HuD staining [pnuc] and a cytoplasmic ROI with positive HuD staining [cyto]) in >30 enteric neurons stained for Ret9 or Ret51 and HuD. The ratio of mean Ret signal intensity (cyto/pnuc) was determined and plotted. Cells were derived from five individual rat pups for each isoform. (D) Retinoic acid–treated SH-SY5Y cells were transiently transfected with the plasma membrane marker EPN1-ENTH-GFP (green), fixed, and stained for RET9 or RET51 (red). Inserts in top left-hand corners are magnifications of the boxed region in the merged panels, highlighting regions of well-defined plasma membrane (arrows). Scale bars, 10 μm in full image, 2 μm in magnification. (E) Mean pixel intensity of the RET and EPN1-ENTH-GFP signals was determined from 3-pixel-wide lines drawn along areas of well-defined plasma membrane where no neighboring cells were present. The ratio of RET9 or RET51/EPN1-ENTH-GFP intensity ($I_{RET}/I_{EPN1\text{-}PH\text{-}GFP}$) for 3-pixel bins was calculated along the entire line and plotted. $n \geq 10$ lines for both RET9 and RET51. *$p < 0.005$.

Because RET9 and RET51 differ exclusively by amino acids in their C-terminal tails, we predicted that these distinct sequences are functionally responsible for differences in isoform localization. To determine whether one or both isoform tails were important for mediating RET maturation and transport to the plasma membrane, we developed two novel RET mutant constructs. First, we replaced the first nine unique amino acids (1064–1072) of RET51 with the corresponding amino acids from RET9 (referred to as 9-in-51; Figure 3B). In the second construct, the RET9 C-terminal amino acids (1064–1072) were added terminally, immediately downstream of the intact RET51 sequence (referred to as 51+9; Figure 3B). Of interest, these two constructs displayed different phenotypes. The 9-in-51 construct displayed a phenotype similar to that of wild-type RET9, appearing predominantly as immature protein, whereas 51+9 showed increased levels of mature protein relative to wild-type RET9, a phenotype identical to that of wild-type RET51 (Figure 3C). This suggests that the RET9 C-terminal amino acid tail, within the context of its normal upstream sequences, is responsible for the retention of this isoform within the Golgi apparatus.

RET51 internalizes more rapidly than RET9

On the basis of our earlier observations that a greater proportion of RET51 is found in the mature 175-kDa form relative to RET9 (Figure 1, B–D) and that RET51 appears to be more abundant in the plasma membrane of SH-SY5Y cells (Figure 2, D and E), we investigated what effect localization may have on activation and internalization of RET9 and RET51 from the cell surface. Initially, we investigated the phosphorylation properties of RET isoforms by immunoprecipitating RET9 and RET51 from SH-SY5Y cell lysates and probing with pan-RET and anti-phosphotyrosine antibodies. As predicted, we found only the mature, 175-kDa band of RET9 and RET51 to be phosphorylated (Figure 4A). Furthermore, the RET51 isoform was relatively more phosphorylated, although a portion of this increase may be due to the additional phosphotyrosines at Y1090 and Y1096 that are not present in RET9 (Figure 1A).

Next, we investigated the movement of RET9 and RET51 into the cell after activation by GDNF using a simple cell surface biotinylation approach. Cells were either left untreated or incubated with GDNF for 20 min, followed by biotinylation of surface proteins, cell

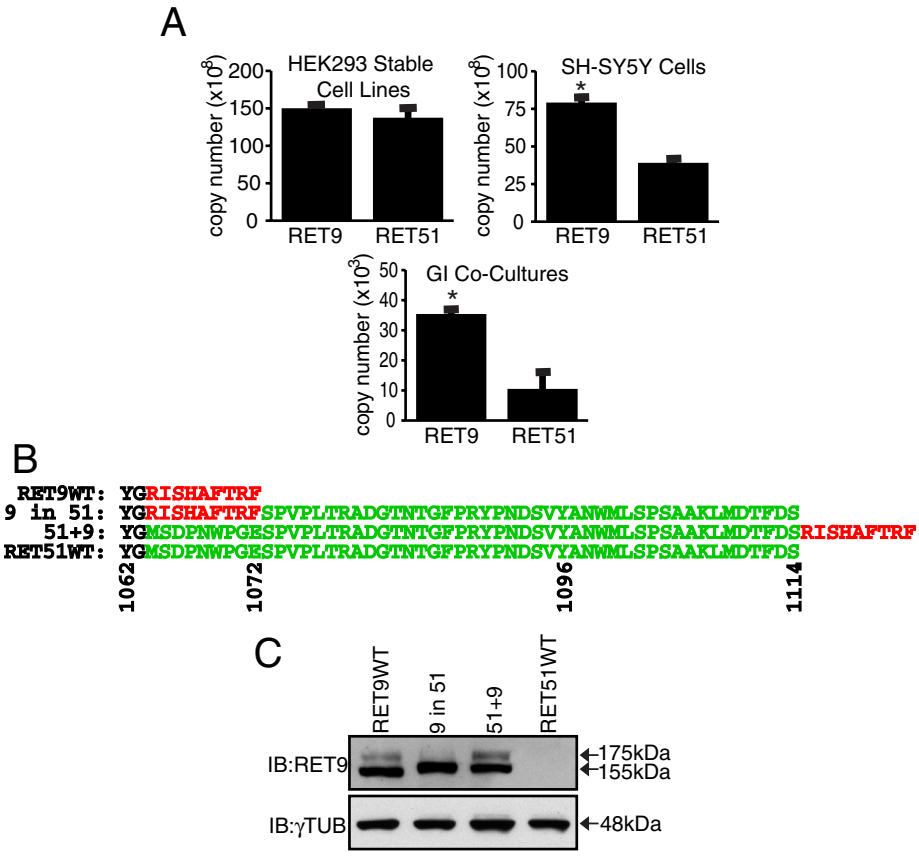

FIGURE 3: The RET9 tail delays maturation. (A) Quantitative real-time PCR was used to determine the approximate copy number of *RET9* and *RET51* transcripts in total RNA samples harvested from the indicated cell lines. Results are means of eight individual measurements from three separate mRNA samples. *$p < .05$ (B) Diagrammatic representation of RET tail mutant constructs used in C. (C) HEK293 cells were transiently transfected with the indicated constructs, cultured for 48 h, harvested, and immunoblotted for RET9 or tubulin.

lysis, and the collection of biotinylated protein on streptavidin-coated beads. As expected, both surface-localized RET9 and RET51 were biotinylated in the absence of GDNF. However, upon GDNF treatment, we observed a greater loss of the surface-localized RET51 (46% of original surface RET51) than RET9 (25% of original surface RET9; Figure 4B)

Biotinylation of cell surface RET in stimulated and unstimulated SH-SY5Y cells was further used to monitor RET internalization over time. Consistent with Figure 4B, Figure 4C shows that both RET isoforms were internalized upon incubation with GDNF, although RET51 internalization was more robust. Thirteen percent of the total surface-localized RET51 was internalized within the first 5 min of GDNF stimulation. However, nearly 30 min of GDNF stimulation was required to internalize a similar fraction of the surface-localized RET9 (16%; Figure 4C). Together these results suggest a more robust and efficient internalization of RET51 in response to GDNF stimulation relative to RET9.

We further investigated RET9 and RET51 trafficking in HeLa cells using a method that combines confocal microscopy, surface biotinylation, and immunofluorescence to observe RET internalization from the plasma membrane and trafficking to the lysosome (Richardson and Mulligan, 2010). This method allowed us to restrict our analyses to the specific subset of intracellular vesicles that had been formed by plasma membrane invagination after addition of GDNF. Thus, we were able to quantify the movement of RET9 and RET51 relative to each other in early endosomes and late endosomes/lysosomes. Consistent with Figure 4C, we observed a more robust internalization of RET51 to early endosomes, relative to RET9 (Figure 4D). Within 5 min of GDNF addition, RET51 was localized to significantly more EEA1-positive endosomes than before GDNF addition ($p < 0.005$; Figure 4D). In comparison, a significant increase in RET9-containing endosomes was achieved only after 30 min of GDNF treatment ($p < 0.005$, Figure 4D). The percentage of early endosomes containing RET9 increased from 0 to 30 min, whereas RET51-containing endosomes reached a maximum by 15 min (Figure 4D; discussed later). At both 15 and 60 min after GDNF addition, RET51 occupied a significantly greater percentage of early endosomes then did RET9 ($p < 0.005$; Figure 4D). Unexpectedly, after 30 min of GDNF treatment, RET51 was present in significantly fewer early endosomes than it was at 15 or 60 min after addition of GDNF ($p < 0.005$, Figure 4D; discussed later).

In addition, the distance of each RET-positive early endosome from the plasma membrane was measured to determine whether RET-positive endosomes trafficked deeper into the cytoplasm over time. Once again, endosomes containing RET51 trafficked significantly deeper into the cytoplasm by 5 min of GDNF treatment (relative to the 0-min time point; $p < 0.005$; Figure 4D), whereas RET9-positive endosomes required 30 min to internalize significantly deeper relative to unstimulated cells ($p < 0.005$; Figure 4D). Furthermore, RET9 endosomes increased their distance from the plasma membrane throughout the entire 60-min time course; however, the mean distance of RET51 endosomes from the plasma membrane was relatively unchanged at time points >15 min (Figure 4D; discussed later).

As expected, both RET isoforms took longer to reach lysosomes (as determined by colocalization with LAMP2) than early endosomes, and, again, a significant increase of RET51 within these structures relative to unstimulated cells was observed earlier than that of RET9 (30 vs. 60 min, respectively; Figure 4D). Again, RET9 colocalization with lysosomes gradually increased throughout the time course, whereas lysosomal localization of RET51 showed little change after 15 min of GDNF treatment (Figure 4D; discussed later).

Isoform-specific recycling of RET51

Our observation that RET51 occupies significantly fewer early endosomes after 30 min of GDNF stimulation (relative to the 15- and 60-min time points; Figure 4C), as well as the apparent lack of its accumulation in early endosomes and lysosomes at time points >15 min, led us to investigate whether RET51 could enter endosomal recycling pathways. We previously used a novel biotinylation assay to provide evidence of RET51 recycling when it is overexpressed in HeLa cells (Richardson and Mulligan, 2010). Using this assay, we observed RET colocalization with cell surface biotin (Supplemental Figure S3). We noted colocalization of RET51

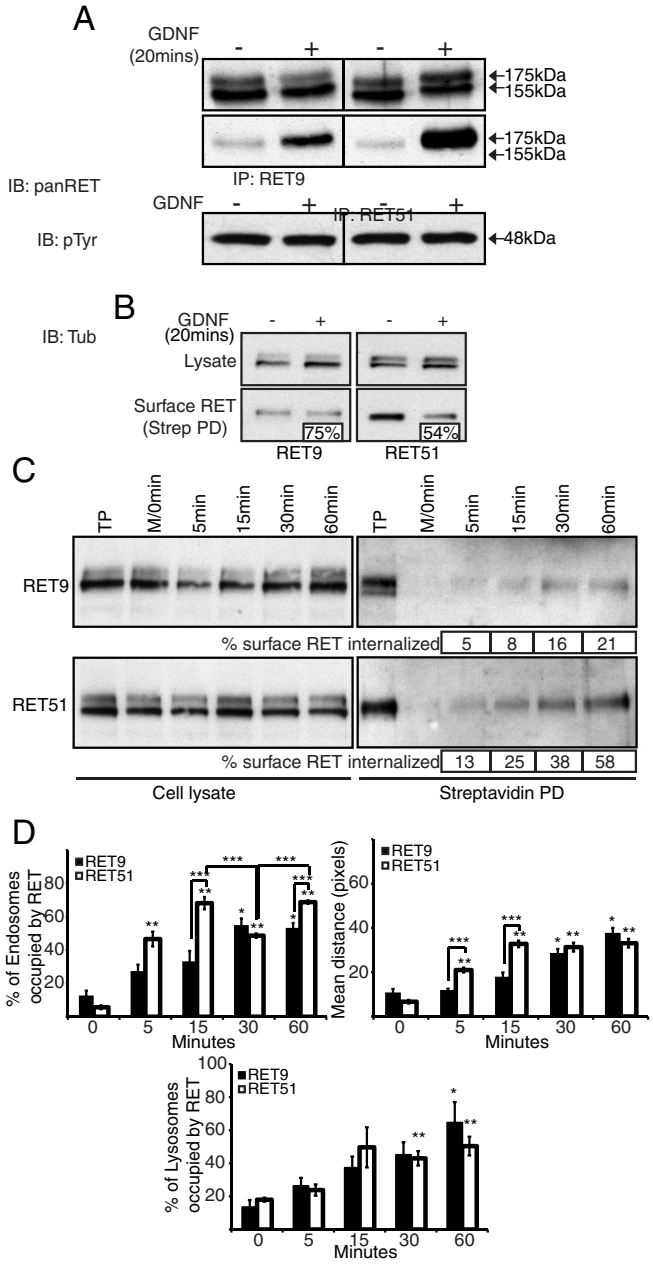

FIGURE 4: RET51 internalizes more efficiently than RET9. (A) Retinoic acid–treated SH-SY5Y cells were serum starved, incubated with or without 100 ng/ml GDNF for 20 min, and lysed. Cell lysates were immunoprecipitated (IP) with antibodies specific to RET9 or RET51, separated by SDS–PAGE, and immunoblotted (IB) with panRET or anti-phosphotyrosine (pTyr) antibodies. A portion of cell lysate was retained and probed with anti–γ-tubulin as a loading control. (B) Retinoic acid–treated SH-SY5Y cells were serum starved, incubated with or without GDNF for 20 min, cooled to 4°C, surface biotinylated, and harvested. Biotinylated proteins were recovered on streptavidin-coated beads and immunoblotted for RET9 or RET51. Densitometry, performed via ImageJ, was used to determine the percentage of the initial surface-localized biotinylated RET remaining after incubation with GDNF as indicated in lower panels. (C) Retinoic acid–treated SH-SY5Y cells were serum starved and surface biotinylated. After biotinylation, cells were returned to 37°C in the presence of 100 ng/ml GDNF for the indicated times before the remaining cell surface biotin was stripped with MeSNa buffer, and cells were lysed. Cell lysates and biotinylated proteins were separated by SDS–PAGE and immunoblotted for RET9 or RET51. TP, total protein control; sample was maintained at 4°C to inhibit internalization and was not stripped with MeSNa buffer. M, MeSNa stripping control; sample was maintained at 4°C to inhibit internalization and subsequently stripped with MeSNa buffer. Densitometry, performed using ImageJ, was used to determine the percentage of the initial surface-localized biotinylated RET recovered via pull-down on streptavidin beads at each time point. (D) HeLa cells, transiently transfected with GFRα1 and RET9 or RET51, were serum starved for 2 h, incubated with CHX for 30 min, and surface biotinylated. Cells were returned to 37°C in the presence of 100 ng/ml GDNF and CHX for the indicated times before fixing and staining for RET, biotin, and EEA1 or LAMP2. The percentage of biotin-labeled endosomes or lysosomes occupied by RET9 or RET51 for each time point was calculated as described in *Materials and Methods* and plotted. Mean distance of RET-containing endosomes, formed after addition of GDNF, from the plasma membrane was determined as described in *Materials and Methods* and plotted. Data are expressed as means ± SE. *$p < 0.005$ to RET9 0 min. **$p < 0.005$ to RET51 0 min. ***$p < 0.005$ between indicated samples. All Western blots are representative of three or more independent experiments.

with cell surface biotin before GDNF addition and after 30 min of incubation with GDNF but not after 15 min of GDNF stimulation (Richardson and Mulligan, 2010; Supplemental Figure S3B). At no time point were we able to observe colocalization between RET9 and cell surface biotin (Supplemental Figure S3A). Using our SH-SY5Y cell model, we expanded on the experiments in Figure 2D to examine the colocalization of RET51 with the plasma membrane marker EPN1-ENTH-GFP at various times after GDNF addition. We found a significant depletion of RET51/EPN1-ENTH-GFP colocalization within 5 min of GDNF addition (Figure 5, A and B). However, colocalization was quickly reestablished by 20 min after GDNF addition. This observation was confirmed via surface biotinylation and Western blotting (Figure 5C). Together, these data clearly demonstrate a portion of RET51 protein recycling back to the plasma membrane after internalization. This observation appears to be consistent across multiple cell lines and under various levels of RET51 expression.

RTKs that undergo recycling, such as epidermal growth factor receptor (EGFR) and MET, have been shown to avoid degradation, resulting in extended signaling potential (reviewed in Parachoniak and Park, 2012). To determine whether recycling prevents degradation of RET51, prolonging its signaling capacity within the membrane and cytosol relative to RET9, we treated primary rat GI cocultures with brefeldin A to block RET maturation. Brefeldin A is an inhibitor of Golgi function that is known to trap nascent peptides in the ER, preventing their delivery to the Golgi (Runeberg-Roos *et al.*, 2007). Brefeldin A addition to rat GI cocultures resulted in an accumulation of immature Ret9, and to a lesser extent immature Ret51, over time, indicating that transport of both Ret isoforms from the ER to Golgi and subsequent glycosylation was blocked (Figure 5D). In contrast, the mature protein band of Ret9 decreased in intensity over time, becoming nearly undetectable by 3 h (Figure 5D). The mature protein band of Ret51 maintained a constant intensity throughout the 3-h time course, indicating greater stability of the mature form of this isoform relative to Ret9 (Figure 5D). To confirm that this result was not due to differences in relative RET9 and RET51 protein concentration or the use of individual antibodies to visualize each isoform, we repeated the experiment in our monoisoformic HEK293 stable cell lines using a pan-RET antibody (Figure 5E). In the presence of brefeldin A and GDNF, the pool of mature RET9 protein was quickly degraded. Levels of mature RET51 decreased more

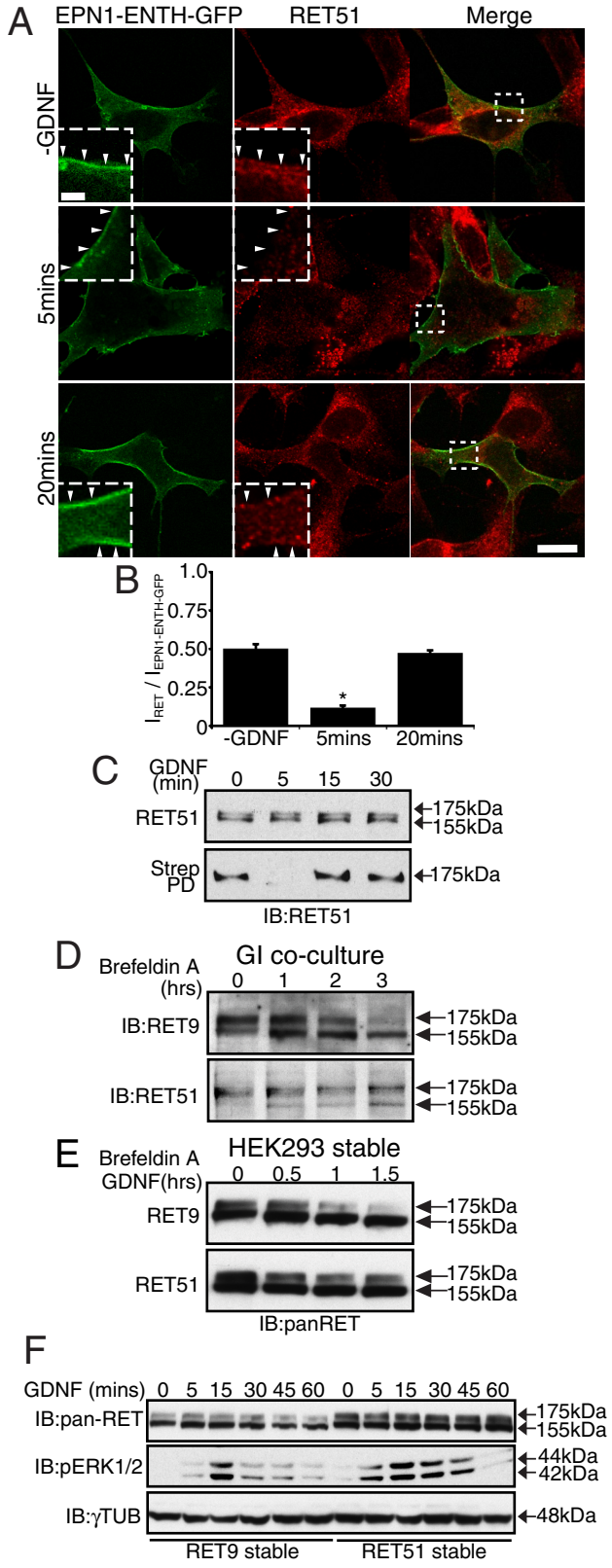

FIGURE 5: RET51 recycles to the plasma membrane. (A) Retinoic acid–treated SH-SY5Y cells were transiently transfected with the plasma membrane marker EPN1-ENTH-GFP (green), incubated with GDNF for the indicated times, fixed, and stained for RET51 (red). Inserts in top or bottom left-hand corners are magnifications of the boxed region in the merged panels, highlighting regions of well-defined plasma membrane (arrows). Scale bars, 10 μm in full image, 2 μm in magnification. (B) Mean pixel intensity of the RET and EPN1-ENTH-GFP signals was determined from 3-pixel-wide lines drawn along areas of well-defined plasma membrane where no neighboring cells were present. The ratio of RET9 or RET51/EPN1-ENTH-GFP intensity ($I_{RET}/I_{EPN1\text{-}PH\text{-}GFP}$) for 3-pixel bins was calculated along the entire line and plotted. $n \geq 10$ lines for both RET9 and RET51. *$p < 0.005$. (C) SH-SY5Y cells were incubated with GDNF for the indicated times and surface biotinylated at 4°C. Cells were lysed, and biotinylated proteins were recovered on streptavidin beads (Strep PD). Both cell lysates and streptavidin pull-downs were separated by SDS–PAGE and immunoblotted for RET51. (D) Rat pup GI cocultures were established as in Figure 1D and grown in DMEM containing 5% FBS. Cells were treated with 5 μg/ml brefeldin A for the indicated times. Cells were lysed and immunoblotted for RET9 or RET51. (E) HEK293 cells stably expressing GFRα1 and RET9 or RET51 were serum starved overnight and treated with 100 ng/ml GDNF and 5 μg/ml Brefeldin A for the indicated times. Cell lysates were immunoblotted for RET using a pan-RET antibody. (F) HEK293 cells stably expressing RET9 or RET51 were serum starved overnight and incubated with GDNF for the indicated times. Cell lysates were immunoblotted using pan-RET, pERK1/2, and tubulin antibodies. Blots are representative of three independent experiments.

slowly, again indicating that this isoform is degraded at a slower rate relative to mature RET9 protein (Figure 5E). Our data are consistent with RET51, but not RET9, being able to recycle back to the plasma membrane after activation and internalization.

Recycling of RTKs has been shown to affect downstream signaling by mediating longer, sustained signaling after ligand binding (Parachoniak and Park, 2012). We previously showed that phosphorylated RET is able to activate the ERK/MAP kinase signaling pathway after internalization from early endosomes within the cytoplasm (Richardson *et al.*, 2006). Therefore, we investigated ERK1/2 signaling downstream of RET9 and RET51 in HEK293 monoisoformic cell lines. Consistent with the more rapid internalization and recycling of the activated RET51 receptor, we found that activation of ERK1/2 initiated earlier and was sustained for a longer duration in RET51-expressing cells than in a RET9-expressing cell line (Figure 5F). This suggests that recycling of RET51 plays an important role in modulating signaling downstream of this isoform. Indeed, recycling of RET51 provides a strong mechanistic explanation for the increased transforming capacity of this isoform.

RET51 recycles through a RAB11-associated pathway

To confirm RET51's presence in a recycling pathway, we performed colocalization studies with various markers of recycling endosomes. Barysch *et al.* (2009, 2010) developed an in vitro system that efficiently sorts cointernalized molecules (e.g., transferrin and low-density lipoprotein) into separate vesicles based on their final destination (e.g., recycling vs. lysosome). We used this system to examine the ability of RET9 and RET51 to be sorted away from transferrin-containing endosomes in postnuclear supernatants (PNSs). Transferrin is a well-characterized small iron-binding, soluble protein (Hopkins, 1983; Hopkins and Trowbridge, 1983; Maxfield and McGraw, 2004). After binding its cell surface receptor, transferrin is rapidly internalized to early endosomes, releases its bound iron molecules, detaches from its receptor, and sorts to recycling endosomes before being exocytosed (Hopkins, 1983; Hopkins and Trowbridge, 1983; Maxfield and McGraw, 2004). PNSs were produced from SH-SY5Y cells that had been stimulated with GDNF for 15 min and Alexa 488–labeled transferrin for 5 min. PNSs were then incubated either on ice or at 37°C for 45 min in the presence of an

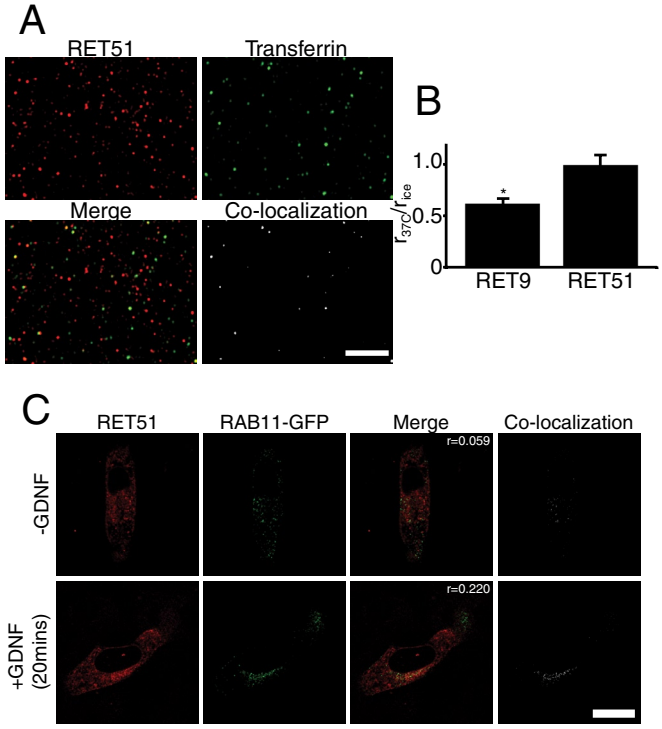

FIGURE 6: RET51 colocalizes with markers of the endosomal-recycling pathway. (A) Retinoic acid–treated SH-SY5Y cells were collected and incubated with GDNF for 10 min and Alexa 488–labeled transferrin for 5 min at 37°C. Postnuclear supernatants were prepared using a ball homogenizer. Samples were either kept on ice or incubated for 45 min in rat-brain cytosol extract at 37°C before attachment to coverslips and fixation in 3% paraformaldehyde. Coverslips were immunostained for RET9 or RET51 and imaged via a wide-field fluorescence microscope. (B) Pearson's *r* was calculated using ImageJ for each image, and the ratio of *r* at 37°C to that at ice temperature (r_{37C}/r_{ice}) was determined and plotted. Data are representative of two independent experiments with four fields of view analyzed in each (~8000 transferrin-positive endosomes). (C) HeLa cells were transiently transfected with RET51 and RAB11-GFP, incubated with 100 ng/ml GDNF where indicated, fixed, and stained for RET51 (red). Pearson's *r* was calculated for each image and is displayed in the Merge panel. Colocalization was determined using ImageJ as indicated in *Materials and Methods*. Images are representative of one of three independent experiments. Scale bars, 10 μm (A), 40 μm (C).

artificial ATP-regenerating system to allow endosomal sorting to occur. After this sorting reaction was completed, endosomes were fixed to coverslips and stained for RET9 or RET51. Values of Pearson's *r* were then calculated for each colocalized image. By comparing *r* from samples incubated on ice to those incubated at 37°C, we calculated the ratio r_{37C}/r_{ice}. As seen in Figure 6B, *r* values for images stained for RET51 were relatively unchanged under the two conditions ($r_{37C}/r_{ice} = 0.99$), whereas RET9 images showed a significant decrease in colocalization after the sorting reaction was completed ($r_{37C}/r_{ice} = 0.62$; $p < 0.05$). This suggests that RET51 remains along with transferrin in the recycling compartment during intracellular sorting, whereas a proportion of RET9 is sorted away from transferrin-containing endosomes.

We next investigated whether RET9 and RET51 were present in recycling vesicles of intact HeLa cells. RAB4 and RAB11 are commonly used markers of recycling endosomes. RAB4 is generally associated with recycling endosomes that rapidly return to the cell surface (van der Sluijs *et al.*, 1992), whereas RAB11 endosomes participate in a slower recycling pathway that involves movement through the endocytic recycling compartment (ERC), a perinuclear collection of RAB11-positive vesicles (Ullrich *et al.*, 1996). We used colocalization studies in whole cells to determine whether RET51 or RET9 colocalized with either of these recycling endosome markers. HeLa cells were transiently transfected with RET9 or RET51 and RAB4-GFP or RAB11-GFP to determine whether RET is found within endosomes decorated with these markers. Both RET9 and RET51 displayed low levels of colocalization with RAB4-positive vesicles that was unchanged after addition of GDNF (Supplemental Figure S4A). Of interest, although cells expressing RET9 showed no changes in their intracellular distribution of RET (Supplemental Figure S4, A and B), GDNF addition to cells expressing RET51 and either RAB4 or RAB11 resulted in a perinuclear accumulation of RET51 (Figure 6C and Supplemental Figure S4A). In cells expressing RET51 and RAB11, strong colocalization was seen between these two proteins at this perinuclear location (Figure 6C). As stated earlier, no GDNF-induced change in RET9 distribution was seen in cells expressing RAB4 or RAB11 (Supplemental Figure S4). In addition, little colocalization was seen between RET9 and RAB11, and RET9 did not display a perinuclear accumulation after GDNF addition (Supplemental Figure S4B). The observation of RET51 in RAB11-positive endosomes further supports our model in which this isoform, and not RET9, is sorted to a recycling pathway. In addition, the perinuclear localization of RET51/RAB11 vesicles resembles the ERC, of which RAB11 is a marker, and suggests that RET51 recycles through the ERC via the slower, RAB11-associated recycling pathway.

DISCUSSION

Until recently, mechanisms of protein trafficking were believed to play passive roles in cellular signaling and metabolism. However, numerous data now show that the processes of exocytosis and endocytosis can modulate the function of transmembrane receptors by controlling their signaling potential in both space and time (reviewed in Sorkin and Von Zastrow, 2002; Cross *et al.*, 2009; Gould and Lippincott-Schwartz, 2009; Parachoniak and Park, 2012). Here we showed that the two most abundant isoforms of RET—RET9 and RET51—display distinct subcellular localizations, trafficking properties, and downstream signaling capacity (summarized in Figure 7) in multiple model cell culture systems and primary rat enteric neurons. These distinct properties may contribute to some of the previously described differences in RET isoform downstream signaling and functional effects and their individual roles in development.

Inefficient maturation of RET9 results in distinct subcellular localizations of RET isoforms

Our data show that *RET* isoforms are coexpressed and that the *RET9* transcript is expressed at higher levels relative to *RET51* in SH-SY5Y cells and the enteric ganglia of neonatal rats. However, this does not translate into higher levels of RET9 protein at the cell surface. Here, we show an accumulation of immature RET9 protein in a perinuclear region that colocalizes with areas of the *trans*-Golgi network (Figure 2, A–C, and Supplemental Figure S1B). Relative to RET51, which is rapidly processed to its mature form, RET9 is present in lower quantities in the plasma membrane (Figure 2, D and E, and Supplemental Figure S3). This suggests that RET9's accumulation in the Golgi limits the amount of functional RET9 receptors at the cell surface (Figure 2, D and E, and Supplemental Figure S3). However, it should be noted that only a relatively minor proportion of both RET9 and RET51 was localized on the plasma membrane (Figure 2, A and D, and Supplemental Figures S1, S3, and S4). Direct visualization

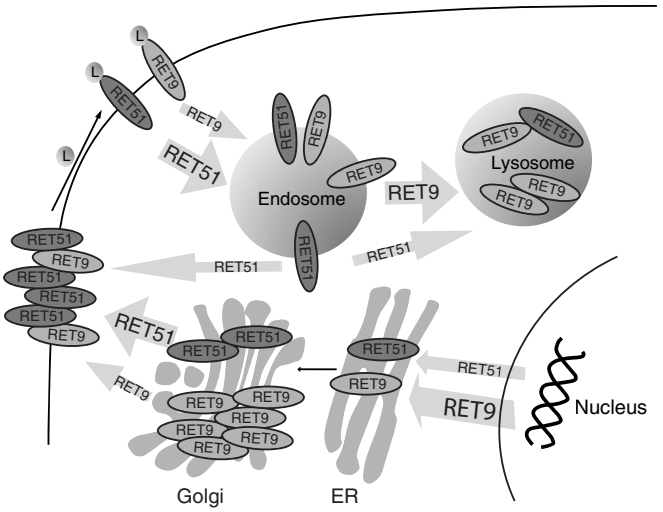

FIGURE 7: Proposed mechanism of RET isoform-specific trafficking. Diagrammatic summary of the data presented here. *RET9* is transcribed at higher levels relative to *RET51*, and both transcripts are delivered to the ER for translation. RET9 and RET51 proceed through the secretory pathway, where RET51 is efficiently delivered to the membrane, whereas a portion of RET9 is retained in the Golgi. On the surface RET9 and RET51 are both able to bind the GDNF/GFRα1 ligand complex (L), autophosphorylate, and activate downstream signaling cascades. After activation RET51 is internalized to endosomes more rapidly than RET9. From endosomes, RET9 is delivered to lysosomes, whereas a portion of RET51 recycles back to the plasma membrane through a RAB11-positive recycling pathway and the rest is targeted to the lysosome. Arrow width is indicative of relative amounts of transcript or protein following each path.

revealed that the majority of both of these molecules were found intracellularly (Figures 2, A and D, and Supplemental Figures S1, S3, and S4).

Recent studies by Hirata *et al*. and Li *et al*. elucidated some important characteristics of RET maturation and trafficking to the plasma membrane. Hirata *et al*. (2010) showed that acidification of the Golgi is required for glycosylation of RET9 and EGFR in this organelle. Of interest, they found initial glycosylation of RET9 (from 120-kDa nascent protein to the 155-kDa immature form) can proceed in the ER when the V-ATPase responsible for vesicle acidification is blocked, and expression of immature RET9 at the plasma membrane can be detected in V-ATPase–inhibited cells (Hirata *et al*., 2010). Another factor that has been shown to affect the ability of RET to traffic through the exocytic pathway is the phosphorylation status of threonine 675 in the juxtamembrane region of RET (Li *et al*., 2012). T675 can be phosphorylated by protein kinase C, and this phosphorylation was found to increase RET levels on the cell surface (Li *et al*., 2012). Although this residue is common to both isoforms and therefore not responsible for the phenotypes noted here, this finding indicates that posttranslational modifications to the cytoplasmically exposed region of RET can affect its transport from the ER and Golgi to the cell surface. Our tail mutant study (Figure 3, B and C) suggests that the RET9 tail, in conjunction with a portion of the RET9 and RET51 shared sequence immediately N-terminal to the tail region, contains posttranslational modifications such as phosphorylation and/or important interactions with cytosolic proteins that regulate the movement of this isoform through the Golgi.

Of interest, RET9 and RET51 heterodimers have not been detected in vivo despite the coexpression of isoforms and their identical extracellular domains (Tsui-Pierchala *et al*., 2002; Scott *et al*., 2005). It has been hypothesized that this was due to targeting of RET9 and RET51 to individual lipid subdomains of the plasma membrane (Tsui-Pierchala *et al*., 2002; Scott *et al*., 2005). Although this may also be a factor, our results suggest that the limited amounts of RET found at the cell surface, the relatively greater concentration of RET51 in the plasma membrane, and the rapid isoform-specific sorting of internalized RET51 to the recycling pathway would minimize the formation of heterodimers and make detection of any heterodimers that do form difficult in vivo.

Isoform-specific trafficking postinternalization

We previously showed that RET is rapidly internalized from the plasma membrane after activation and observed constitutively active, membrane-bound RET proteins in various structures of the endocytic pathway (Richardson *et al*., 2006, 2009). Here, our analyses of these processes in an isoform-specific context revealed two key differences between RET9 and RET51 intracellular trafficking: the rapid internalization of RET51 relative to RET9 (Figure 4) and the ability of RET51 to recycle to the membrane after internalization, whereas RET9 is targeted to the lysosome (Figures 4–7).

The mechanisms underlying the recycling of plasma membrane proteins are poorly understood. It was postulated that membrane proteins were continuously recycled to the cell surface in the absence of ubiquitination through a rapid, short-loop recycling pathway (Dunn *et al*., 1989; Mayor *et al*., 1993; Katzmann *et al*., 2002). More recently, a number of targeting motifs have been identified within various non-RTK membrane proteins that direct their recycling back to the plasma membrane (Johnson *et al*., 2001; Wang *et al*., 2004; Paasche *et al*., 2005). This motif-based receptor recycling appears to be a lengthier process, as endocytosed receptors are first sorted to the ERC before returning to the membrane via a long-loop recycling pathway (Johnson *et al*., 2001). MET and EGFR are the best-understood RTKs with regard to their recycling properties (reviewed in Parachoniak and Park, 2012). MET recycling appears to be directed by the ARF-binding protein GGA3, which is recruited to MET upon activation by its ligand HGF. GGA3 binding occurs in the early endosome and initiates MET trafficking into RAB4-positive recycling vesicles, which are predominantly associated with the rapid, short-loop recycling pathway (Parachoniak *et al*., 2011). Of interest, knockout of GGA3 inhibited MET recycling and led to a reduction in ERK1/2 signaling, suggesting that recycling plays an important role in sustaining downstream signaling from MET (Parachoniak *et al*., 2011). EGFR recycling appears to be more complex, in that it has been shown to occur through both rapid, short-loop recycling and the long-loop, ERC-associated pathway (reviewed in Sorkin and Goh, 2009). Extracellular ligand concentration and dissociation of ligand from EGFR within the early endosome appear to be the major determinants of whether EGFR is targeted for recycling or degradation (Sigismund *et al*., 2008; Sorkin and Goh, 2009; Parachoniak *et al*., 2011). Our results indicate that RET51 can be found in both RAB4-positive (short loop) and RAB11-positive (long loop) endosomes, suggesting a recycling mechanism similar to that for EGFR. However, the GDNF-induced increase of RET51 colocalization with RAB11 and its accumulation in a perinuclear ERC-like structure suggest that RET51 is predominantly recycled through the long-loop pathway (Figure 6C; Ullrich *et al*., 1996). On the basis of our observation that RET51 undergoes GDNF-induced colocalization with RAB11, a marker of motif-based recycling and the ERC, we predict that the RET51 tail contains a yet-unidentified recycling motif that mediates its return to the plasma membrane via this pathway.

Tsui and Pierchala (2010) recently investigated retrograde signal propagation downstream of RET in primary sympathetic and sensory neurons. They showed that GDNF applied directly to axonal tips and not the cell body sustained neuronal survival in dorsal root ganglion (DRG) sensory neurons but not in superior cervical ganglion (SCG) sympathetic neurons, which are seen to rapidly apoptose (Tsui and Pierchala, 2010). Tsui and Pierchala provided two possible explanations for these observations. First, they suggested that the increased levels of RET9 in DRG neurons allow for a stronger survival signal to be conveyed to the cell body, and, second, they observe a more rapid degradation of RET51 in the axons of SCG neurons relative to DRG neurons. Our data, along with previous studies that highlight RET51's relatively higher transforming and signaling capacity, indicate that the more rapid loss of RET51 from the axonal tips of SCG neurons may be the key determinant in the different phenotypes of SCG and DRG neurons observed by Tsui and Pierchala. However, because these are vastly different systems (DRG, SCG, enteric neurons, cultured SH-SY5Y cells), one must be careful in drawing parallels between the data. Perhaps more important, together these data clearly indicate that RET can play different roles in different cell lineages and highlight the importance of the use of specific primary tissues in the validation of experimental observations.

Degradation of RET9 and RET51

Previous studies used the translation inhibitor cycloheximide (CHX) to evaluate RET protein stability (Scott *et al.*, 2005; Pierchala *et al.*, 2006; Richardson *et al.*, 2009). Using this method, Pierchala *et al.* (2006) and Scott *et al.* (2005) showed RET9 to be more stable than RET51 in primary sympathetic neurons and monoisoformic stable cell lines. We believe that the brefeldin A investigations presented here (Figure 5) complement these previous studies by providing further insight into the translation, posttranslational processing, trafficking, and degradation of RET isoforms. In the cell models investigated here, when Golgi function is impaired by brefeldin A and the transport of immature RET to the plasma membrane is blocked, RET9 is degraded more rapidly than RET51, as it cannot recycle (Figure 5D). We hypothesize that in CHX studies, which assess total intracellular and surface-bound RET protein, the large pool of immature RET9 within the exocytic pathway (Figure 1, B–D) continues to mature in the presence of CHX, increasing the overall perceived stability of total RET9 protein relative to RET51. Therefore our data suggest that the time required for maturation of the immature RET9 pool, its delivery to the plasma membrane, internalization, and degradation may be responsible for the previously observed greater stability of RET9 relative to RET51 in CHX-based assays.

It is well established that wild-type and oncogenic mutant forms of RET51 proteins have greater transforming and differentiation-inducing ability relative to similar wild-type and mutant RET9 proteins in cell-based assays (colony formation, fibroblast transformation, PC12 cell differentiation; Pasini *et al.*, 1997; Rossel *et al.*, 1997; Iwashita *et al.*, 1999; Le Hir *et al.*, 2000). RET51's ability to recycle and avoid degradation may contribute to this greater transforming ability. Recycling of RET51 increases its residency within the plasma membrane and cytoplasm relative to RET9, prolonging its time in the two regions of the cell where initiation of RET signal transduction is most active (Richardson *et al.*, 2006). Here we showed that recycling of RET51 leads to more rapid and prolonged ERK1/2 activation from this isoform relative to signaling downstream of RET9. In addition, a study of primary pheochromocytoma tumors containing activating *RET* mutations previously showed increased levels of *RET51* transcript relative to normal tissues, whereas *RET9* transcript levels remained constant (Le Hir *et al.*, 2000). This may indicate that increased expression of RET51, but not of RET9, is selected for during tumor development. Our model suggests that a relative increase in RET51 levels would be a more advantageous growth-promoting alteration for the cell due to the increased amounts of cell surface protein and the slower degradation of the RET51 isoform relative to RET9.

Conclusions

Here we presented a comprehensive study of the subcellular localization and intracellular trafficking of RET receptor isoforms in multiple cell models. Intracellular trafficking is known to have important roles in downstream signaling from membrane receptors. Not only does it provide a mechanism for ablating these signals, but it also provides additional mechanisms for modulating and targeting signals originating from membrane receptors both spatially and temporally. Our data indicate that differential subcellular localizations and trafficking properties of RET isoforms result in distinct localizations and degradative properties of RET9 and RET51 that may affect the signaling capacities of these isoforms. Alternative splicing is now recognized as a key step in evolution, allowing a single gene to encode multiple proteins with differing functions. Substitution of 9 or 51 unique amino acids at the C-terminal tail of RET is a striking example of the effect that alternative splicing can have on subcellular trafficking and localization of proteins within the cell.

MATERIALS AND METHODS

Cell culture and transfections

HeLa, HEK293, and SH-SY5Y cells were cultured in DMEM with 10% fetal bovine serum (FBS; Sigma-Aldrich, Oakville, Canada). Retinoic acid, 10 μM, was added to SH-SY5Y cells 24 h before each experiment to induce RET expression. Transient transfections were performed using Lipofectamine 2000 (Invitrogen, Burlington, Canada) with previously described plasmids encoding GFRα1, RET9, RET51, RAB4-GFP, and RAB11-GFP (Gujral *et al.*, 2006; Johns *et al.*, 2009). EPN1-ENTH-GFP was cloned by inserting cDNA encoding EGFP and two copies of the ENTH domain of EPN1 (amino acids 130–243 of isoform A) in-frame into the pcDNA3.1+ mammalian expression vector (Invitrogen). EPN1 cDNA was obtained from Open Biosystems (Lafayette, CO). The 9-in-51 and 51+9 constructs were developed by PCR-based, site-directed mutagenesis of RET51 cDNA. The 9-in-51 construct was created by mutating the first nine unique codons (encoding amino acids 1064–1072) of the RET51 tail to the corresponding sequence from RET9. The 9+51 construct was created by inserting the same RET9 tail coding sequence directly 3′ of the unique RET51 tail. Neonatal rat GI cocultures, consisting of myenteric neurons, glia, and smooth muscle cells, were obtained from 4-d-old Sprague Dawley rats (Charles River, Wilmington, MA) as previously described (Rodrigues *et al.*, 2011). Briefly, the smooth muscle and myentric plexus layers were peeled from the entire length of the small intestine. This tissue was minced, digested with 0.125% trypsin II and 0.5 mg/ml collagenase F (Sigma-Aldrich) in Hank's solution buffered with 4-(2-hydroxyethyl)-1-piperazineethanesulfonic acid, and plated in DMEM containing 5% FBS (Sigma-Aldrich), 5 mg/ml soybean trypsin inhibitor (Sigma-Aldrich), and 2 mg/ml ciprofloxacin (Bayer, Wayne, NJ). Cells were allowed to adhere for ~60 h, the final 12 h without serum, where indicated. GDNF (PeproTech, Rocky Hill, NJ), cycloheximide (BioShop, Burlington, Canada), and brefeldin A (BioShop) were added where indicated at final concentrations of 100 ng/ml, 100 μg/ml, and 5 μg/ml, respectively.

Immunoblotting

SDS–PAGE and immunoblotting were performed as previously described (Richardson *et al.*, 2009) using the antibodies and dilutions outlined in Supplemental Table S1.

Quantitative real-time PCR

Quantitative real-time PCR was performed as described previously (Richardson *et al.*, 2009). Briefly, standard curves were obtained by plotting crossing threshold (*Ct*) values for serial dilutions of linearized *RET* cDNA (human or rat). The *Ct* values for 200 ng of total RNA, isolated from HEK293, SH-SY5Y, or rat GI cocultures using TRIzol (Invitrogen), were obtained and fitted to the standard curves to determine the approximate copy number of *RET* transcripts in each sample. The RET isoform-specific primer pairs CRT14B/KRT14D (RET9) and CRT14B/KRT20A (RET51) have been previously described (Ivanchuk *et al.*, 1997). For cells of rat origin, corresponding rat sequence primers KRT14Drat (GTTACAGACAGTTGGGATGGT) and KRT20Arat (ATCGGCTCTCGTGAGTGGT) were used in conjunction with CRT14B (conserved sequence in human and rat).

Immunofluorescence

Immunofluorescence was performed as described previously (Richardson *et al.*, 2009; Richardson and Mulligan, 2010), with the following modifications: for GI coculture studies, glass coverslips were coated with 20 ng/ml bovine collagen, and HeLa cells were plated on coverslips coated with 0.2% gelatin. Antibodies, and concentrations used are summarized in Supplemental Table S1. Biotinylated proteins were detected with Alexa 594–conjugated streptavidin (Invitrogen) diluted 1:200 in 3% bovine serum albumin (BSA; wt/vol) in phosphate-buffered saline (PBS). Nuclei were visualized with Hoechst 33342 diluted 1:1000 in 3% BSA (wt/vol) in PBS.

Biotinylation

Biotinylation of cells for assessment of membrane vesicle trafficking and recycling of membrane proteins has been extensively described (Richardson and Mulligan, 2010). To quantify total surface RET, cells were serum starved overnight, incubated with or without 100 ng/ml GDNF (PeproTech) for 20 min, washed twice in PBS, cooled to 4°C, and biotinylated as previously described (Smith *et al.*, 2004). Cells were lysed, and biotinylated protein was recovered using streptavidin-coated beads (Invitrogen), followed by separation by SDS–PAGE before immunoblotting. To determine the amount of internalized RET, cells were serum starved and biotinylated as described. After biotinylation, culture medium containing 100 ng/ml GDNF was added to cells, and they were returned to 37°C for various amounts of time. Cells were again washed with cold PBS and cooled to 4°C, and the remaining surface biotin was stripped with 50 mM MeSNa buffer (two washes of 15 min). Cells were lysed, and biotinylated protein was recovered, as described.

Quantitation of relative signal intensity in confocal images

ImageJ (Abramoff et al., 2004) was used to calculate the average signal intensity in circular regions of interest (ROIs) in the cytosol of primary enteric neurons or along 3-pixel-wide linear ROIs on sections of SH-SY5Y cell plasma membrane. Mean pixel intensities were determined for each channel of an ROI, and ratios of those signal intensities were calculated.

Quantitation of RET-containing vesicles

The percentage of endosomes or lysosomes occupied by RET9 or RET51 was determined by counting the number of vesicles in which RET, biotin, and either EEA1 or LAMP2, respectively, colocalized and dividing by the total number of vesicles counted in the EEA1 or LAMP2 channel. A vesicle was defined as an object >10 pixels in size in which each pixel had an intensity >10 (using a standard 8-bit pixel intensity scale of 0–255). These objects were counted using the ImageJ Analyze Particles function (Abramoff et al., 2004). Triple colocalization of RET, biotin, and EEA1 or LAMP2 was determined using the ImageJ (National Institutes of Health, Bethesda, MD) RG2B Colocalization (developed by Christopher Philip Mauer, Northwestern University, Chicago, IL) plug-in for ImageJ (Abramoff et al., 2004). First, a hybrid image of the biotin and EEA1 or LAMP2 channels was produced in which any pixel that did not meet our colocalization criteria was replaced with a zero-intensity (black) pixel. To be considered colocalized, a pixel had to have an intensity >10 in both channels and the intensity of the biotin signal had to be within 60% of EEA1/LAMP2, or vice versa. If a pixel met these criteria, it was replaced by a gray-scale pixel with intensity equal to the mean of the two channels. The hybrid image was then colocalized to the corresponding RET channel in the same manner to produce a final image representing the colocalization of all three channels.

Determining endosome distance from membrane

The triple-colocalization images (produced as just described) were remerged with the corresponding biotin channel. The distance in pixels from each endosome in the triple-colocalization image to the nearest portion of plasma membrane (visualized by the biotin signal) was calculated using ImageJ and plotted.

In vitro endosome-sorting assay

This protocol was previously published in detail (Barysch *et al.*, 2010). Briefly, SH-SY5Y cells were treated with retinoic acid overnight, collected into a conical tube, and incubated with GDNF for 10 min, followed by addition of Alexa 488–labeled transferrin for 5 min at 37°C. Cells were placed on ice and washed repeatedly with PBS. Postnuclear supernatants were prepared using a custom-built ball homogenizer. Samples were divided into two lots and either kept on ice or incubated for 45 min in rat brain cytosol extract at 37°C in the presence of an ATP-regenerating system (as described by Barysch *et al.*, 2010). Cells were again cooled on ice before attachment to coverslips by centrifugation and fixation in 3% paraformaldehyde. Coverslips were immunostained for RET9 or RET51 (as described here and in Supplementary Table 1) using isoform-specific primary antibodies and a Cy3-labeled secondary antibody and imaged using a Leica (Wetzlar, Germany) wide-field fluorescence microscope. Images from the RET9 or RET51 and transferrin channels were overlaid, and Pearson's coefficients of colocalization were calculated using the Mander's coefficients plug-in for ImageJ (developed by Tony Collins, Wright Cell Imaging Facility, Toronto, Canada; Abramoff et al., 2004). Data are representative of two independent experiments with four fields of view analyzed in each (~8000 transferrin-containing endosomes).

Statistical analysis

All data are expressed as means ± SE. A two-tailed, unpaired Student's *t* test was used to determine statistical significance.

ACKNOWLEDGMENTS

We thank Stephen Ferguson for his kind gift of the RAB4- and RAB11-GFP constructs. We also thank Jeffrey Mewburn, Matthew Gordon, and Jalna Meens (Queen's Cancer Research Institute Imaging Facility, Kingston, Canada) for valuable input and Judy Vanhorne for technical assistance. This work was supported by an operating grant from the Canadian Institutes for Health Research (L.M.M.;

MOP49602). D.S.R. was supported by a Terry Fox Foundation Studentship through the National Cancer Institute of Canada and is a fellow of the Alexander von Humboldt Society. B.D.H. was supported by a fellowship from the Terry Fox Foundation Training Program in Transdisciplinary Cancer Research in Partnership with Canadian Institutes for Health Research.

REFERENCES

Abramoff MD, Magelhaes PJ, Ram SJ (2004). Image processing with ImageJ. Biophot Int 11, 36–42.

Airaksinen MS, Saarma M (2002). The GDNF family: signalling, biological functions and therapeutic value. Nat Rev Neurosci 3, 383–394.

Amiel J, Lyonnet S (2001). Hirschsprung disease, associated syndromes, and genetics: a review. J Med Genet 38, 729–739.

Arighi E, Borrello MG, Sariola H (2005). RET tyrosine kinase signaling in development and cancer. Cytokine Growth Factor Rev 16, 441–467.

Asai N, Murakami H, Iwashita T, Takahashi M (1996). A mutation at tyrosine 1062 in MEN2A-Ret and MEN2B-Ret impairs their transforming activity and association with shc adaptor proteins. J Biol Chem 271, 17644–17649.

Barlow A, de Graaff E, Pachnis V (2003). Enteric nervous system progenitors are coordinately controlled by the G protein-coupled receptor EDNRB and the receptor tyrosine kinase RET. Neuron 40, 905–916.

Barysch SV, Aggarwal S, Jahn R, Rizzoli SO (2009). Sorting in early endosomes reveals connections to docking- and fusion-associated factors. Proc Natl Acad Sci USA 106, 9697–9702.

Barysch SV, Jahn R, Rizzoli SO (2010). A fluorescence-based in vitro assay for investigating early endosome dynamics. Nat Protoc 5, 1127–1137.

Besset V, Scott RP, Ibanez CF (2000). Signaling complexes and protein-protein interactions involved in the activation of the Ras and phosphatidylinositol 3-kinase pathways by the c-Ret receptor tyrosine kinase. J Biol Chem 275, 39159–39166.

Burry RW, Smith CL (2006). HuD distribution changes in response to heat shock but not neurotrophic stimulation. J Histochem Cytochem 54, 1129–1138.

Burzynski G, Shepherd IT, Enomoto H (2009). Genetic model system studies of the development of the enteric nervous system, gut motility and Hirschsprung's disease. Neurogastroenterol Motil 21, 113–127.

Cosma MP, Cardone M, Carlomagno F, Colantuoni V (1998). Mutations in the extracellular domain cause RET loss of function by a dominant negative mechanism. Mol Cell Biol 18, 3321–3329.

Cross BC, Sinning I, Luirink J, High S (2009). Delivering proteins for export from the cytosol. Nat Rev Mol Cell Biol 10, 255–264.

de Graaff E, Srinivas S, Kilkenny C, D'Agati V, Mankoo BS, Costantini F, Pachnis V (2001). Differential activities of the RET tyrosine kinase receptor isoforms during mammalian embryogenesis. Genes Dev 15, 2433–2444.

De Vita G, Melillo RM, Carlomagno F, Visconti R, Castellone M, Bellacosa A, Billaud M, Fusco A, Tsichlis PN, Santoro M (2000). Tyrosine 1062 of RET-MEN2A mediates activation of Akt (protein kinase B) and mitogen-activated protein kinase pathways leading to PC12 cell survival. Cancer Res 60, 3727–3731.

Dunn KW, McGraw TE, Maxfield FR (1989). Iterative fractionation of recycling receptors from lysosomally destined ligands in an early sorting endosome. J Cell Biol 109, 3303–3314.

Encinas M, Crowder RJ, Milbrandt J, Johnson EM Jr (2004). Tyrosine 981, a novel ret autophosphorylation site, binds c-Src to mediate neuronal survival. J Biol Chem 279, 18262–18269.

Ford MG, Mills IG, Peter BJ, Vallis Y, Praefcke GJ, Evans PR, McMahon HT (2002). Curvature of clathrin-coated pits driven by epsin. Nature 419, 361–366.

Gould GW, Lippincott-Schwartz J (2009). New roles for endosomes: from vesicular carriers to multi-purpose platforms. Nat Rev Mol Cell Biol 10, 287–292.

Gujral TS, Singh VK, Jia Z, Mulligan LM (2006). Molecular mechanisms of RET receptor-mediated oncogenesis in multiple endocrine neoplasia 2B. Cancer Res 66, 10741–10749.

Gujral TS, van Veelen W, Richardson DS, Myers SM, Meens JA, Acton DS, Dunach M, Elliott BE, Hoppener JW, Mulligan LM (2008). A novel RET kinase-beta-catenin signaling pathway contributes to tumorigenesis in thyroid carcinoma. Cancer Res 68, 1338–1346.

Hayashi H *et al*. (2000). Characterization of intracellular signals via tyrosine 1062 in RET activated by glial cell line-derived neurotrophic factor. Oncogene 19, 4469–4475.

Heanue TA, Pachnis V (2008). Ret isoform function and marker gene expression in the enteric nervous system is conserved across diverse vertebrate species. Mech Dev 125, 687–699.

Hickey JG, Myers SM, Tian X, Zhu SJ, JL VS, Andrew SD, Richardson DS, Brettschneider J, Mulligan LM (2009). RET-mediated gene expression pattern is affected by isoform but not oncogenic mutation. Genes Chromosomes Cancer 48, 429–440.

Hirata Y, Shimokawa N, Oh-hashi K, Yu ZX, Kiuchi K (2010). Acidification of the Golgi apparatus is indispensable for maturation but not for cell surface delivery of Ret. J Neurochem 115, 606–613.

Hopkins CR (1983). Intracellular routing of transferrin and transferrin receptors in epidermoid carcinoma A431 cells. Cell 35, 321–330.

Hopkins CR, Trowbridge IS (1983). Internalization and processing of transferrin and the transferrin receptor in human carcinoma A431 cells. J Cell Biol 97, 508–521.

Ivanchuk SM, Eng C, Cavenee WK, Mulligan LM (1997). The expression of RET and its multiple splice forms in developing human kidney. Oncogene 14, 1811–1818.

Ivanchuk SM, Myers SM, Mulligan LM (1998). Expression of RET 3′ splicing variants during human kidney development. Oncogene 16, 991–996.

Iwashita T *et al*. (1999). Biological and biochemical properties of Ret with kinase domain mutations identified in multiple endocrine neoplasia type 2B and familial medullary thyroid carcinoma. Oncogene 18, 3919–3922.

Jain S, Encinas M, Johnson EM Jr, Milbrandt J (2006). Critical and distinct roles for key RET tyrosine docking sites in renal development. Genes Dev 20, 321–333.

Johns HL, Berryman S, Monaghan P, Belsham GJ, Jackson T (2009). A dominant-negative mutant of rab5 inhibits infection of cells by foot-and-mouth disease virus: implications for virus entry. J Virol 83, 6247–6256.

Johnson AO, Lampson MA, McGraw TE (2001). A di-leucine sequence and a cluster of acidic amino acids are required for dynamic retention in the endosomal recycling compartment of fibroblasts. Mol Biol Cell 12, 367–381.

Katzmann DJ, Odorizzi G, Emr SD (2002). Receptor downregulation and multivesicular-body sorting. Nat Rev Mol Cell Biol 3, 893–905.

Kjaer S, Ibanez CF (2003). Intrinsic susceptibility to misfolding of a hot-spot for Hirschsprung disease mutations in the ectodomain of RET. Hum Mol Genet 12, 2133–2144.

Kramer ER, Aron L, Ramakers GM, Seitz S, Zhuang X, Beyer K, Smidt MP, Klein R (2007). Absence of Ret signaling in mice causes progressive and late degeneration of the nigrostriatal system. PLoS Biol 5, e39.

Lai AZ, Gujral TS, Mulligan LM (2007). RET signaling in endocrine tumors: delving deeper into molecular mechanisms. Endocr Pathol 18, 57–67.

Le Hir H, Charlet-Berguerand N, Gimenez-Roqueplo A, Mannelli M, Plouin P, de Franciscis V, Thermes C (2000). Relative expression of the RET9 and RET51 isoforms in human pheochromocytomas. Oncology 58, 311–318.

Lee KY, Samy ET, Sham MH, Tam PK, Lui VC (2003). 3′ Splicing variants of ret receptor tyrosine kinase are differentially expressed in mouse embryos and in adult mice. Biochim Biophys Acta 1627, 26–38.

Li XZ, Yan J, Huang SH, Zhao L, Wang J, Chen ZY (2012). Identification of a key motif that determines the differential surface levels of RET and TrkB tyrosine kinase receptors and controls depolarization enhanced RET surface insertion. J Biol Chem 287, 1932–1945.

Lorenzo MJ, Gish GD, Houghton C, Stonehouse TJ, Pawson T, Ponder BAJ, Smith DP (1997). REt alternative splicing influences the interaction of activated RET with the SH2 and PTB domains of Shc, and the SH2 domain of Grb2. Oncogene 14, 763–771.

Maxfield FR, McGraw TE (2004). Endocytic recycling. Nat Rev Mol Cell Biol 5, 121–132.

Mayor S, Presley JF, Maxfield FR (1993). Sorting of membrane components from endosomes and subsequent recycling to the cell surface occurs by a bulk flow process. J Cell Biol 121, 1257–1269.

Myers SM, Mulligan LM (2004). The RET receptor is linked to stress response pathways. Cancer Res 64, 4453–4463.

Paasche JD, Attramadal T, Kristiansen K, Oksvold MP, Johansen HK, Huitfeldt HS, Dahl SG, Attramadal H (2005). Subtype-specific sorting of the ETA endothelin receptor by a novel endocytic recycling signal for G protein-coupled receptors. Mol Pharmacol 67, 1581–1590.

Parachoniak CA, Luo Y, Abella JV, Keen JH, Park M (2011). GGA3 functions as a switch to promote Met receptor recycling, essential for sustained ERK and cell migration. Dev Cell 20, 751–763.

Parachoniak CA, Park M (2012). Dynamics of receptor trafficking in tumorigenicity. Trends Cell Biol 22, 231–240.

Park HJ, Mylvaganum M, McPherson A, Fewell SW, Brodsky JL, Lingwood CA (2009). A soluble sulfogalactosyl ceramide mimic promotes Delta

F508 CFTR escape from endoplasmic reticulum associated degradation. Chem Biol 16, 461–470.
Pasini A, Geneste O, Legrand P, Schlumberger M, Rossel M, Fournier L, Rudkin BB, Schuffenecker I, Lenoir GM, Billaud M (1997). Oncogenic activation by two distinct *FMTC* mutations affecting the tyrosine kinase domain. Oncogene 15, 393–402.
Pierchala BA, Milbrandt J, Johnson EM Jr (2006). Glial cell line-derived neurotrophic factor-dependent recruitment of Ret into lipid rafts enhances signaling by partitioning Ret from proteasome-dependent degradation. J Neurosci 26, 2777–2787.
Ponnambalam S, Girotti M, Yaspo ML, Owen CE, Perry AC, Suganuma T, Nilsson T, Fried M, Banting G, Warren G (1996). Primate homologues of rat TGN38: primary structure, expression and functional implications. J Cell Sci 109, Pt 3, 675–685.
Richardson DS, Gujral TS, Peng S, Asa SL, Mulligan LM (2009). Transcript level modulates the inherent oncogenicity of RET/PTC oncoproteins. Cancer Res 69, 4861–4869.
Richardson DS, Lai AZ, Mulligan LM (2006). RET ligand-induced internalization and its consequences for downstream signaling. Oncogene 25, 3206–3211.
Richardson DS, Mulligan LM (2010). Direct visualization of vesicle maturation and plasma membrane protein trafficking. J Fluoresc 20, 401–405.
Rodrigues DM, Li AY, Nair DG, Blennerhassett MG (2011). Glial cell line-derived neurotrophic factor is a key neurotrophin in the postnatal enteric nervous system. Neurogastroenterol Motil 23, e44–e56.
Rossel M *et al*. (1997). Distinct biological properties of two RET isoforms activated by MEN 2A/FMTC and MEN 2B mutations. Oncogene 14, 265–275.
Runeberg-Roos P, Virtanen H, Saarma M (2007). RET(MEN 2B) is active in the endoplasmic reticulum before reaching the cell surface. Oncogene 26, 7909–7915.
Schuchardt A, D'Agati V, Larsson-Blomberg L, Costantini F, Pachnis V (1994). Defects in the kidney and enteric nervous system of mice lacking the tyrosine kinase receptor Ret. Nature 367, 380–383.
Schuetz G, Rosario M, Grimm J, Boeckers TM, Gundelfinger ED, Birchmeier W (2004). The neuronal scaffold protein Shank3 mediates signaling and biological function of the receptor tyrosine kinase Ret in epithelial cells. J Cell Biol 167, 945–952.
Schuringa JJ, Wojtachnio K, Hagens W, Vellenga E, Buys CH, Hofstra R, Kruijer W (2001). MEN2A-RET-induced cellular transformation by activation of STAT3. Oncogene 20, 5350–5358.
Scott RP, Eketjall S, Aineskog H, Ibanez CF (2005). Distinct turnover of alternatively spliced isoforms of the RET kinase receptor mediated by differential recruitment of the Cbl ubiquitin ligase. J Biol Chem 280, 13442–13449.
Sigismund S, Argenzio E, Tosoni D, Cavallaro E, Polo S, Di Fiore PP (2008). Clathrin-mediated internalization is essential for sustained EGFR signaling but dispensable for degradation. Dev Cell 15, 209–219.
Smith CA, Dho SE, Donaldson J, Tepass U, McGlade CJ (2004). The cell fate determinant numb interacts with EHD/Rme-1 family proteins and has a role in endocytic recycling. Mol Biol Cell 15, 3698–3708.
Sorkin A, Goh LK (2009). Endocytosis and intracellular trafficking of ErbBs. Exp Cell Res 315, 683–696.
Sorkin A, Von Zastrow M (2002). Signal transduction and endocytosis: close encounters of many kinds. Nat Rev Mol Cell Biol 3, 600–614.
Sorkin A, von Zastrow M (2009). Endocytosis and signalling: intertwining molecular networks. Nat Rev Mol Cell Biol 10, 609–622.
Tahira T, Ishizaka Y, Itoh F, Sugimura T, Nagao M (1990). Characterization of *ret* proto-oncogene mRNAs encoding two isoforms of the protein product in a human neuroblastoma cell line. Oncogene 5, 97–102.
Takahashi M, Buma Y, Taniguchi M (1991). Identification of the *ret* proto-oncogene products in neuroblastoma and leukemia cells. Oncogene 6, 297–301.
Tsui CC, Pierchala BA (2010). The differential axonal degradation of Ret accounts for cell-type-specific function of glial cell line-derived neurotrophic factor as a retrograde survival factor. J Neurosci 30, 5149–5158.
Tsui-Pierchala BA, Ahrens RC, Crowder RJ, Milbrandt J, Johnson EM Jr (2002). The long and short isoforms of ret function as independent signaling complexes. J Biol Chem 277, 34618–34625.
Ullrich O, Reinsch S, Urbe S, Zerial M, Parton RG (1996). Rab11 regulates recycling through the pericentriolar recycling endosome. J Cell Biol 135, 913–924.
van der Sluijs P, Hull M, Webster P, Male P, Goud B, Mellman I (1992). The small GTP-binding protein rab4 controls an early sorting event on the endocytic pathway. Cell 70, 729–740.
van Weering DH, Moen TC, Braakman I, Baas PD, Bos JL (1998). Expression of the receptor tyrosine kinase Ret on the plasma membrane is dependent on calcium. J Biol Chem 273, 12077–12081.
Wang X, Ma D, Keski-Oja J, Pei D (2004). Co-recycling of MT1-MMP and MT3-MMP through the *trans*-Golgi network. Identification of DKV582 as a recycling signal. J Biol Chem 279, 9331–9336.